Macromolecules 2019, 52, 8275–8284

Unconventional Complex Coacervation between Neutral Polymer and Inorganic Polyoxometalate in Aqueous Solution via Direct **Water Mediation**

Benxin Jing,*,† Manuela Ferreira,† Yunyi Gao,‡ Christopher Wood,† Ruipeng Li,§ Masafumi Fukuto,§ Tianbo Liu, to and Yingxi Zhu*, to

Supporting Information



ABSTRACT: Water, specifically in a hydration shell, is critical for many biological supramolecular aggregations in nature, where water can directly mediate intermolecular association via hydrogen bonding and is regarded as "structured water". Conversely, little has been reported on the biomimetic water-mediated supramolecular assembly with adequately high water content to date, because of the competing thermodynamic processes of water hydration and water as a building block to participate in self-assembly. In this work, we explore water-mediated complexation based on entropy-driven biphasic coacervate formation using highly hydrophilic neutral polymer and inorganic mineral-analogous nanoclusters. For the first time (to the best of our knowledge), nonelectrostatic liquid-liquid separating coacervate formation is demonstrated between polyethylene glycol (PEG) and polyoxometalate (POM) nanoclusters in aqueous solutions of varied PEG and POM concentrations, POM types, and aqueous medium conditions. Comprehensive characterization using fluorescence microscopy, small-angle X-ray scattering, calorimetry, and other techniques has confirmed that the compositions, microstructure, and thermodynamics of PEG-POM complex coacervation are highly similar to entropy-driven complex coacervation between oppositely charged polyelectrolytes in aqueous solution. However, the effect of heavy water on critical POM concentration for the onset of coacervate formation suggests that water, instead of the counter ions as commonly debated for polyelectrolyte complex coacervation, is responsible for PEG-POM coacervate formation. Specifically, structured water works as a hydrogen bond donor for both highly hydrated PEG and POM to directly mediate the PEG-water-POM association, resulting in the release of excess hydrated water for entropy-driven PEG-POM complex coacervation. Therefore, water-mediated complex coacervation could be developed as a general and simple strategy to build biomimetic hybrid nanomaterials with high water content for various applications from energy-related functional nanomaterials to biomedical ramification.

INTRODUCTION

Water plays critical roles in many supramolecular assemblies in nature as well as synthetic complex functional materials. In addition to the common notion that water is the "life's solvent", water is an active building block in cells and many other biological complexes.^{1,2} In past decades, it has been widely reported that water could directly mediate intermolecular interactions via hydrogen bonding for many biological activities, such as stabilizing protein conformations and protein-DNA and ligand-receptor complexation,³⁻⁹ controlling protein aggregation and amyloid fibrization, 10 constructing bone apatite, 17,12 and facilitating the transport of protons and

oxygen molecules during photosynthesis. 13 Such functional water is generally considered as "structured water" to be distinct from bulk water.^{2,14} As inspired by the role of structured water in biology, many material scientists have explored water as the building block for biomimetic supramolecular assembly and polymerization. 15,16 Yet, because of the competing functions of water as both a solvent and a building constitute in such material processes, ¹⁷ one grand

Received: May 28, 2019 Revised: September 2, 2019 Published: October 25, 2019

Department of Chemical Engineering and Materials Science, Wayne State University, Detroit, Michigan 48202, United States

[‡]Department of Polymer Science, The University of Akron, Akron, Ohio 44325, United States

[§]National Synchrotron Light Source II, Brookhaven National Laboratory, Upton, New York 11973, United States

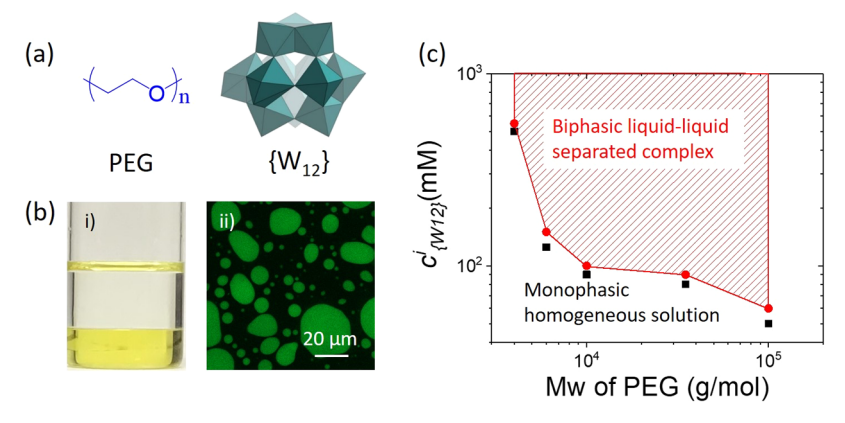


Figure 1. (a) Molecular structures of PEG and lithium metatungstate, $\{W_{12}\}$, (b) digital photograph (i) and fluorescence micrograph (ii) of PEG- $\{W_{12}\}$ complex coacervate formed at $c_{\{W_{12}\}}^i = 200$ mM, $c_{EG}^i = 1.135$ M and $c_{LiCl}^i = 2.0$ M, for which 10 wt % f-PEG over total PEG weight is added to the PEG-100k aqueous solution before mixing with $\{W_{12}\}$ aqueous solution. The micrograph was acquired by CLSM with an Airy detector. The scale bar is 20 μm as shown in (ii). (c) Effect of PEG molecular weight (M_w) on the phase diagram of PEG- $\{W_{12}\}$ complex formation as characterized by CLSM. At constant initial $c_{EG}^i = 1.135$ M and $c_{LiCl}^i = 2.0$ M, critical $\{W_{12}\}$ concentration, $c_{\{W_{12}\}}^i$ (red circles) for the onset of liquid-liquid separated PEG- $\{W_{12}\}$ coacervate formation (red shaded region) is plotted against PEG M_w . At $c_{\{W_{12}\}}^i < c_{\{W_{12}\}}^i$ the mixture of PEG-LiCl and $\{W_{12}\}$ solution exhibits a monophasic homogeneous solution (black squares).

challenge in artificial supramolecular aggregates is to achieve adequately high water content comparable to that in human and animal bodies. ¹⁸

One particular biomimetic supramolecular complex that could contain high water content (>80 wt %) is polymeric complex coacervate. Complex coacervates are a special family of supramolecular complexes formed in water, for which all the components are highly water-soluble, but the mixture of their aqueous solutions spontaneously separates into two liquid phases at given concentrations and temperature. They are commonly present in living cells¹⁹ and the organisms of sea animals such as mussels and sandworms^{20–22} and have also been linked to the origin of life. 23,24 Recently, biomimetic complex coacervates have been developed as underwater adhesives, 25 supramolecular assemblies, 26,27 self-healing hydrogels,²⁸ drug/gene delivery,²⁹ and artificial protocells.^{30,31} Among them, most complex coacervates are formed between oppositely charged polyelectrolytes in salted water via electrostatic interaction, 32-35 while a few others are formed via cation $-\pi$ and zwitterion—anion interactions. ^{36–39} Surprisingly, despite its importance and abundant presence of water in biological complex coacervates, little work on biomimetic complex coacervation resulting from direct nonelectrostatic water mediation have been reported to date yet. The difficulty in using water to bind two, or more than two, distinct polymeric solutes in aqueous solution might arise from the following dilemma: water-solute interaction (hydration), which is accounted for the solutes to be dissolved or dispersed in water, leads to entropy gain, while supramolecular complexation, which results from the aggregation between distinct solutes, often leads to entropy penalty. However, as water-mediated biomolecular aggregation exists in nature, we simply question how to manipulate water molecules and control water-mediated supramolecular aggregation. One possibility is to explore the entropy-driven complex coacervation, where entropy gain is often achieved by releasing counter ions near macro-ions to the bulk aqueous solution. It should be noted that the negative enthalpy change resulting from intermolecular attraction and association is not required in the case of entropy-driven complex coacervation. Thus, we

hypothesize that entropy-driven coacervate formation could be also achieved by releasing a large number of interfacial hydration water, instead of counter ions, near macro-ions or highly hydrophilic polymers to bulk aqueous solution, thereby compensating the entropy penalty upon complexation. To test this hypothesis, we intentionally avoid any ion pairing between the charged polyelectrolytes in aqueous medium to minimize any contribution from the electrostatic interaction. As structured water is commonly present in many biological and highly hydrophilic polymers, bone, and even minerals, 3-9,11,12,40,41 we choose a neutral hydrophilic polymer and highly water-soluble mineral analogue nanoclusters as two building constitutes to examine water-mediated complexation in aqueous solution, considering a huge number of water molecules in the hydration shell surrounding them. 42-44 Such organic-inorganic hybrid complexes are also advantageous to further modify the material properties of individual components and integrate their functionalities over a wide range for broad applications.

Specifically, in this work we choose polyethylene glycol (PEG) as the hydrophilic polymer component, which is one of the simple, neutral, and biocompatible polymers with high solubility in water and each of whose monomer is associated with approximately one hydration water molecule. 45 PEG has been used as a hydrogen bond acceptor to form hydrogenbonding complexes over decades. 46,47 We choose the polyoxometalate (POM) nanocluster as the inorganic watersoluble mineral analogue. POM is the nanocluster of transition-metal oxides, $\{MO_n\}_{n=0}^{48}$ where n=4-7 and M is generally Mo, W, V, U, and Nb in well-defined crystalline structures, often carries stable and well-defined multiple negative charges over its typical nanocluster size of 1-6 nm in aqueous solution. POM has recently emerged as novel functional nanomaterials for various applications from catalysis to medicines. 48,49 Because it is highly charged, POM is highly hydrated and surrounded by a large number of water molecules in aqueous solution.⁵⁰ Additionally, it is recently reported that POMs typically contain two types of structured water molecules including confined and coordinated water, both of which play critical roles in the stability and maintaining the

architectural framework of POMs. 31,51,52 In this work, we mainly focus on Keggin ion-like lithium metatungstate, $\text{Li}_6\text{H}_2\text{W}_{12}\text{O}_{40}$ ($\{W_{12}\}$), while other similar POMs are also investigated to verify the general complex coacervation with PEG as discussed in Supporting Information. Herein, we explore the nonelectrostatic complex coacervation between PEG and $\{W_{12}\}$ in aqueous solutions of varied PEG chain length, PEG and $\{W_{12}\}$ concentrations, and aqueous medium conditions, from which the role of water in the origin of PEG– $\{W_{12}\}$ complex coacervation is investigated.

EXPERIMENTAL SECTION

Materials and Sample Preparation. PEG of $M_{\rm w}=4000,\,6000,\,10\,000,\,35\,000,\,$ and $100\,000\,$ g/mol (denoted as PEG-4k, 6k, $10k,\,35k,\,$ and $100k,\,$ respectively), lithium chloride (LiCl), silver nitrate (AgNO₃), and deuterium oxide (D₂O) were all purchased from Sigma-Aldrich and used directly. Aqueous solution of $\{W_{12}\}$, whose molecular structure is shown in Figure 1a, was purchased from LMT liquid and freeze-dried (Labconco FreeZone 4.5 freeze dryer) before experiments. Other POMs used in this work were also commercial available and their sample preparation was detailed in Supporting Information. Amine end-functionalized methoxy PEG (PEG-NH₂) of $M_{\rm w}=35\,300\,$ g/mol was purchased from Jenkem Technology USA and fluorescence labeled by fluorescein-5-isothiocyanate (FITC, Invitrogen) and purified by dialysis in deionized water (Barnstead Smart2Pure) to obtain fluorescent PEG (f-PEG).

PEG– $\{W_{12}\}$ complex coacervation was mainly investigated by mixing 100 g/L PEG (EG monomer concentration $c_{\rm EG}^i=2.27$ M) of a given $M_{\rm w}$ in 4.0 M LiCl aqueous solution with equal volume of $\{W_{12}\}$ aqueous solution of varied concentration from 10 to 800 mM, while other PEG and LiCl concentrations were also varied and examined in this work. All the aqueous solutions used in this work were prepared by using 1.0 mL Eppendorf pipette with its volume uncertainty < 0.005 mL.

Characterization. Phase behavior and morphological structure of PEG– $\{W_{12}\}$ complexes in LiCl solution were examined by a confocal laser scanning microscope (CLSM, Carl Zeiss LSM 800) using a 63× objective lens (Plan Apochromat, NA = 1.4, oil immersion) and an Airyscan detector (Carl Zeiss), in which f-PEG was added at a f-PEG/PEG weight ratio of 1:9. All the characterization reported in this work was carried out at constant temperature, T=22 °C.

 $\{W_{12}\}\$ concentration in the dense coacervate and supernatant phase was determined by the respective density in each phase based on the calibrated density of {W₁₂}-LiCl aqueous solution. The density of {W₁₂}-LiCl aqueous solution is linearly proportional to the concentration of $\{W_{12}\}$ over the range of 50 mM < $c_{\{W_{12}\}}$ < 800 mM, corresponding to the effective density of {W₁₂}-LiCl aqueous solution 1.10 g/cm³ < ρ < 2.95 g/cm^{3.53} Such conditions were satisfied in this work. The sensitivity of $\{W_{12}\}$ concentration measurement can be achieved at the level of ~4.0 mM corresponding to the density change of 0.01 g/cm³ in {W₁₂} aqueous solution, which could be readily determined by weighing 1.0 mL solution using an analytical balance with precision 0.1 mg. It is noted that the presence of the PEG polymer in either coacervate or supernatant phase shows negligible effect on the effective density of the overall solution because of its comparable density to that of water.⁵⁴ LiCl concentration in the supernatant and coacervate phase was determined by titrating Clusing AgNO₃ with K₂CrO₄ as an indicator (aka, the Mohr's method). 55,56 The Mohr's method is known as an extremely sensitive and accurate method to determine chlorine concentration with a relative standard deviation $\leq 0.07\%$. ⁵⁷ All the reported results were obtained with repeated experiments for 5-10 times with samples prepared under the same conditions.

Enthalpy change upon PEG–{ W_{12} } complexation at T=22 °C was determined by isothermal titration calorimetry (ITC, Nano ITC, TA Instruments). Experimentally, 26 consecutive aliquots of each 10 μ L { W_{12} }–LiCl mixed solution of $c_{\{W_{12}\}}=200$ mM and $c_{\text{LiCl}}=2.0$ M were injected into a 1.1 mL liquid cell filled with 950 μ L PEG–LiCl mixed

solution of $c_{\rm PEG} = 5.0$ g/L and $c_{\rm LiCl} = 2.0$ M. Subsequent injection of $\{W_{12}\}$ was carried out at a time interval of 400 s. A constant stirring speed of 250 rpm was maintained throughout the experiment to ensure sufficient mixing after each injection.

The microscopic structure of PEG– $\{W_{12}\}$ complex coacervates was characterized by small-angle X-ray scattering (SAXS) with incident X-ray wavelength, $\lambda=0.0729$ nm (X-ray energy of 17 keV) using a Pilatus 2M detector (Dectris, Baden-Dättwil, Switzerland) at the Complex Materials Scattering (CMS/11-BM) beamline of the National Synchrotron Light Source II (NSLS-II), Brookhaven National Laboratory (BNL). The distance between the coacervate sample and the SAXS detectors was 5 m, which was calibrated using silver behenate with the first-order reflection at a scattering vector of q=1.076 nm⁻¹, where $q=(4\pi\sin\theta)/\lambda$ with θ being the half-scattering angle. The data acquisition time for each SAXS pattern was 30 s.

RESULTS AND DISCUSSION

Complex Coacervate Formation between Neutral PEG Polymer and POM in Aqueous Solution. We start with determining the phase diagram of PEG-{W₁₂} complexation in LiCl solution. In this work, LiCl is selected as the added salt simply because the solubility of $\{W_{12}\}$ in water is the highest and least affected by added LiCl in comparison to other common salts such as NaCl and KCl. We observe that at a constant initial concentration of total EG monomers of PEG of different $M_{\rm w}$ in the final mixture, $c_{\rm EG}^{\rm i} = 1.135$ M, PEG-{W₁₂} biphasic complex coacervate can be formed by mixing PEG-LiCl and {W₁₂}-LiCl aqueous solution when the initial total $\{W_{12}\}$ concentration, $c_{\{W_{12}\}}^i$ in the final mixture exceed a critical value, $c_{\{W_{12}\}}^c$, which depends on PEG M_w as shown in Figure 1. It is noted that no coacervate formation is observed at the initial total LiCl concentration, c_{LiCl}^{i} < 2.0 M for PEG of varied $M_{\rm w}$ and varied $c_{\{W_{12}\}}^{i}$. Upon mixing, the mixture appears cloudy and spontaneously separates into two clear aqueous liquid phases. Below the critical concentrations, a clear monophasic solution is observed after mixing without any visible phase separation over several months. To verify the coacervate formation, we add FITC-labeled f-PEG to the mixture. As the photograph is shown in Figure 1b(i), the yellow-colored bottom phase in the glass vial clearly indicates that the majority of PEG is present in the dense phase upon liquid-liquid phase separation in contrast to the nearly colorless dilute supernatant phase on the top. Furthermore, the formation and biphasic signature morphology of PEG-{W₁₂} complex coacervates in LiCl aqueous solution is also confirmed by CLSM. As shown in Figure 1b(ii), fluorescent droplets of the polymer-rich phase are dispersed in the nonfluorescent supernatant solution of the polymer-poor phase and could show coalescence over time, confirming the hallmark of liquid-liquid separating complex coacervate.

The formation of PEG– $\{W_{12}\}$ complex coacervate strongly depends on the $M_{\rm w}$ of PEG and $c_{\{W_{12}\}}^{\rm i}$ in the aqueous mixture. As the phase diagram for PEG– $\{W_{12}\}$ coacervate formation is shown in Figure 1c, at constant $c_{\rm EG}^{\rm i}=1.135$ M and $c_{\rm LiCl}^{\rm i}=2.0$ M, $c_{\{W_{12}\}}^{\rm c}$, above which complex coacervates are formed, decreases with increasing PEG $M_{\rm w}$, suggesting that a longer PEG chain facilitates the formation of PEG– $\{W_{12}\}$ complex coacervate better than shorter chains. Such $M_{\rm w}$ -dependence appears similar to that of conventional coacervate formation between oppositely charged polyelectrolytes, where increasing $M_{\rm w}$ of polyelectrolytes broadens the coacervate region. S8–60 It is generally considered that for conventional polyelectrolyte

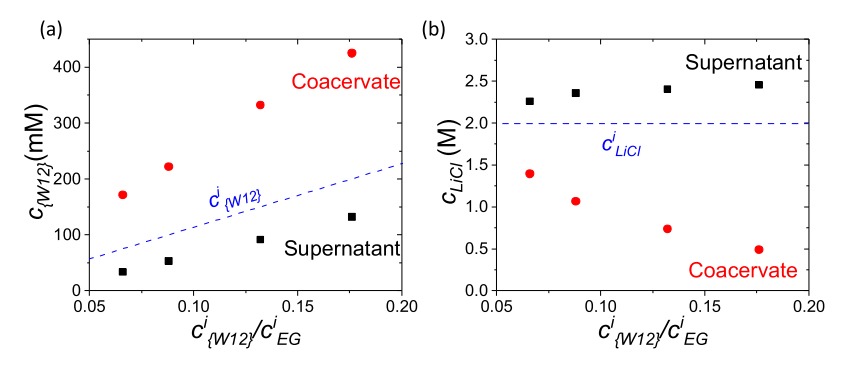


Figure 2. Measured molar concentrations of (a) $\{W_{12}\}$ and (b) LiCl in the supernatant (black squares) and dense phase (red circles) of biphasic PEG- $\{W_{12}\}$ complexes against initial $\{W_{12}\}$ -to-EG monomer molar concentration ratio, $c_{\{W_{12}\}}^i/c_{EG}^i$, in comparison to their respective initial concentration in the mixture (blue dash line), for which PEG-100k at $c_{EG}^i = 1.135$ M is used.

complex coacervation, enhanced cooperative interactions with reduced translational entropy is accounted for broadening the coacervate phase for longer polymer chains than shorter ones. However, the overall monotonic change of the phase diagram as shown in Figure 1c appears drastically different from the bell-shaped phase diagram for conventional coacervate formation between oppositely charged polyelectrolytes or between polyzwitterions and anionic POMs: 39,61 a peak in a polyelectrolyte or polyzwitterion-to-POM concentration ratio is observed at a given salt concentration and decreasing or increasing the concentration ratio leads to the instability of complex coacervates. In sharp contrast, we observe high stability of PEG-{W₁₂} complex coacervates without the biphasic-to-monophasic transition with increasing $c_{\{W_{i,j}\}}^{i}/c_{EG}^{i}$. It is noted that due to the solubility limit of $\{W_{12}\}$ (~0.8 M in LiCl aqueous solution), $c_{\{W_1\}}^i/c_{EG}^i$ could not exceed 35% at c_{EG}^i = 1.135 M to allow us to examine the instability regime of PEG-{W₁₂} complex coacervates at significantly high $c_{\{W_{12}\}}^1/c_{EG}^1$. Alternatively, the instability regime could be possibly approached by a significantly lowering PEG concentration at fixed $c_{\{W_{12}\}}^1$, yet it becomes conversely difficult in determining the biphasic coacervate formation in the highly dilute polymer solution.

Similar complex coacervation is also observed between PEG and other highly water-soluble POMs, such as silicotungstic acid ($H_4SiW_{12}O_{40}$) and phosphomolybdic acid ($H_3PMo_{12}O_{40}$) as discussed in Supporting Information. Although some of these dense complex coacervates may not appear liquid-like observed by the naked eyes, the coalescence of spherical droplets in supernatant solution with contrasting fluorescence color over time is shown in Figure S1, confirming the liquid nature of the dense phase. Importantly, the generality of PEG–POM coacervate formation is verified.

Compositions of PEG– $\{W_{12}\}$ Complex Coacervates. Both the CLSM image and digital photograph in Figure 1b clearly indicate that the majority of PEG is present in the coacervate phase upon liquid–liquid separating complex coacervation. To further understand PEG– $\{W_{12}\}$ association upon phase separation, we quantify the concentration of $\{W_{12}\}$ and LiCl in the supernatant and dense phases as shown in Figure 2a,b, respectively. $\{W_{12}\}$ concentration is simply determined by solution density calibrated by the known linear concentration—density relationship of $\{W_{12}\}$ aqueous solution in the presence of LiCl due to negligible density of water and PEG in comparison to that $(\sim 3.7 \text{ g/cm}^3)$ of $\{W_{12}\}$. LiCl

concentration is determined by Cl⁻ titration using the Mohr's method with AgNO₃.55 As shown in Figure 2a, {W₁₂} in the initial mixture mostly participates in the dense coacervate phase in contrast to the presence of LiCl mostly in the supernatant phase; combined with the observation in Figure 1b, it seems reminiscent of entropy-driven complex coacervation accompanied with the exclusion of simple ions from the dense phase as observed in polycation-polyanion, 62,63 POM-polyzwitterion,³⁹ nonionic polymer-salt mixture,⁶⁴ and nonionic polymer/polyelectrolyte⁶⁵ complex coacervates. However, it is noted that LiCl concentration in the coacervate phase is much lower than the initial one, suggesting little impact of LiCl on PEG- $\{W_{12}\}$ complexation. Moreover, $c_{\{W_{12}\}}^c$ decreases with increasing circle as shown in Figure S2b, suggesting the facilitation of LiCl for PEG-POM coacervate formation in contrast to salt-induced instability and redissolution of polyelectrolyte complex coacervates.^{39,61} Consistent with a recent report of the salt effect on the complexation of the PEG oligomer with POM,666 we believe a high amount of LiCl is critical to screen the charges of highly charged {W₁₂} of 0.8 nm in diameter and thereby weaken electrostatic repulsion between {W₁₂} nanoclusters to facilitate PEG- $\{W_{12}\}$ aggregation. It also explains why no PEG- $\{W_{12}\}$ complex coacervate is observed at c_{LiCl}^i < 2.0 M. The lower salt concentration in the coacervate phase than that in the supernatant phase could result from the excluded volume of small ions at high concentration, ^{62,63} yet it may be worthy of further investigation in the future.

The composition analysis indicates that PEG– $\{W_{12}\}$ complex coacervate is essentially different from the well-known aqueous two phase system (ATPS) including PEG–salt ATPS. In conventional ATPS, one liquid phase is enriched with respect to one polymer, the other phase is enriched with respect to the second polymer or salt. However in this work, both PEG and $\{W_{12}\}$ are enriched in the coacervate phase, suggesting a distinct phase separation mechanism with ATPS. This is also the major difference of ATPS from complex coacervates.

Nanostructure of PEG–{W₁₂} Complex Coacervate. With the presence of a large number of {W₁₂} in the dense coacervate phase, we examine the microscopic organization of {W₁₂} in PEG–{W₁₂} complex coacervate by SAXS. As SAXS intensity profiles are shown in Figure 3, all the PEG–{W₁₂} mixtures in 2.0 M LiCl solution at different phases, including PEG–{W₁₂} monophasic solution at $c_{\{W_{12}\}}^i < c_{\{W_{12}\}}^c$, separated dilute supernatant, and dense coacervate phases of PEG–

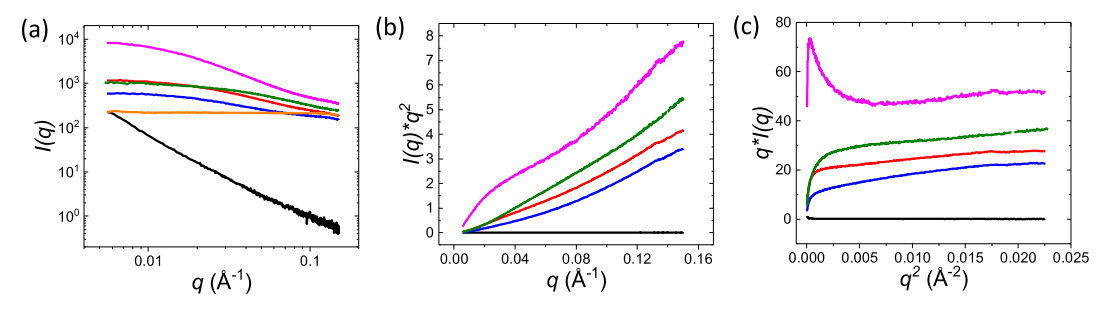


Figure 3. (a) SAXS intensity, I(q), after being normalized by transmission and background subtraction, of PEG- $\{W_{12}\}$ complexes in aqueous media using PEG-100k at constant $c_{\rm EG}^i = 1.135$ M and $c_{\rm LiCl} = 2.0$ M, including monophasic homogeneous mixed solution at $c_{\{W_{12}\}}^i = 40$ mM (red line), supernatant phase (blue line), and dense coacervate (magenta line) of the biphasic complex formed at $c_{\{W_{12}\}}^i = 60$ mM, dense coacervate (green line) of the biphasic complex formed at $c_{\{W_{12}\}}^i = 100$ mM, in comparison to those of $\{W_{12}\}$ -free PEG-LiCl solution (black line) and PEG-free $\{W_{12}\}$ -LiCl solution of $c_{\{W_{12}\}} = 30$ mM (orange line), both of which $c_{\rm LiCl}^i = 2.0$ M. (b) Kratky plot of $I(q) \times q^2$ against q, and (c) GPA of $q \times I(q)$ against q^2 for the cases shown in (a).

{W₁₂} complex coacervates, clearly exhibit a much higher scattering intensity and different intensity profiles in a low q regime (0.01-0.15 Å⁻¹) in comparison to those of PEG-free {W₁₂}-LiCl solution and {W₁₂}-free PEG-LiCl solution as the controls. It should be noted that the scattering intensity of PEG- $\{W_{12}\}\$ complexes mainly results from $\{W_{12}\}\$, as evident from its much higher scattering intensity than that of $\{W_{12}\}$ free PEG solution because of a much higher atomic number of tungsten. Moreover, q-dependent intensity profiles of PEG- $\{W_{12}\}\$ complexes, which are distinct from and far exceed that of PEG-free {W₁₂}-LiCl solution (see orange line in Figure 3a) at low q, strongly suggest the presence of PEG- $\{W_{12}\}$ complex clusters in aqueous mixtures. Surprisingly, the elevated intensity profile of PEG-{W₁₂} monophasic solution also suggests that PEG-{W₁₂} complexes are already formed at $c_{\{W_{12}\}}^{_1} < c_{\{W_{12}\}}^{^c}$ before phase separation, consistent with the SAXS results of PEG oligomer complexation with POM.⁶⁶

To examine the nanostructure of PEG- $\{W_{12}\}$ complex coacervates, we have conducted Kratky analysis ^{67,68} as shown Figure 3b and Porod and Porod-Debye analysis 67,68 in Figure S3. The Kratky plot of $I(q)q^2$ against q is used to qualitatively examine the flexibility and/or degree of unfolding of scattering objects such as particles, macromolecules, and their complexes.^{67–69} For example, a bell-shape Kratky plot suggests a globular and compact structure of scattering objects, while a linear increase with q in a high q regime indicates a random coil-like and loose structure. As shown in Figure 3b, all the PEG- $\{W_{12}\}$ samples exhibit a nearly linear increase of $I(q)q^2$ with q in a high q regime, suggesting a random coil-like and loose structure of PEG- $\{W_{12}\}$ complex clusters, similar to polymers in dilute solution.⁶⁹ To quantify the characteristic size, that is, the gyration radius, R_g of PEG- $\{W_{12}\}$ complex clusters in the dense coacervate phase, we have carried out the Guinier peak analysis (GPA) as shown in Figure 3c.⁷⁰ GPA analysis is used to transform the Guinier region to exhibit a peak to validate the subsequent Guinier analysis to yield R_{σ} ; if no clear peak is observed, the Guinier approximation cannot be applied to the SAXS results. In this work, only for the complex coacervates formed at $c_{\{W_{12}\}}^1$ in close approximation to $c_{\{W_{12}\}}^c$, a clear peak in the GPA plot is observed at $q^2 = 2.88 \times 10^{-4} \text{ Å}^{-2}$, suggesting a relatively uniform size of PEG-{W₁₂} complex clusters. The slope (=1685 Å²) of logarithmic I(q) against q^2 over the q range from 0.013 to 0.024 Å⁻¹ yields $R_g = 7.1$ nm for PEG- $\{W_{12}\}$ complex clusters as the slope is equal to $-R_g^2/3$

according to the Guinier approximation. 71,72 As $c_{\{W_{i}\}}^{i}$ is increased to further evolve PEG– $\{W_{12}\}$ complex coacervation, PEG-{W₁₂} clusters are expected to grow with a looser structure and increased size distribution due to the electrostatic repulsion between {W₁₂} themselves, leading to the disappearance of the peak. Thus, the SAXS results suggest that PEG-{W₁₂} complex coacervates consist of loose aggregates of PEG- $\{W_{12}\}\$ complex clusters with an average size of several nanometers. It should be noted that PEG is found to remain highly mobile in the complex coacervates as verified by fluorescence recovery after photobleaching measurements using f-PEG as the probe (see Figure S4), where the fluorescence intensity of added f-PEG could be 100% recovered after photobleaching. It thus suggests that PEG-{W₁₂} complex coacervates exhibit an intriguing liquid-like behavior, rather than a gel-like one,³⁸ which warrants further investigation.

Role of Water in PEG-{W₁₂} Binding. All the phase behavior, composition, and SAXS structural characterization of biphasic PEG-{W₁₂} complexes consistently indicate that the dense phase is the PEG and {W₁₂}-rich phase while the dilute supernatant solution is the PEG and {W₁₂}-poor phase, further confirming PEG- $\{W_{12}\}$ complex coacervation. The following questions are thereby raised: what is the intermolecular interaction responsible for PEG-{W₁₂} binding? How does water impact the binding? First, we have excluded several common noncovalent interactions in aqueous media that have been reported to be responsible for the supramolecular assembly or complex coacervation, such as charge-charge interaction, π effect, and hydrophobic interaction simply because PEG is uncharged and nonconjugated and $\{W_{12}\}$ is highly hydrophilic without hydrophobic domains. One might argue the role of protons in the center of $\{W_{12}\}$ for its complexation with PEG, however no evidence has shown that these protons could interact with any other molecules when the intermolecular distance across the "thick" tungstate wall is sufficiently large, resulting in negligible van der Waals (vdW) interaction. The titration curve of $\{W_{12}\}$ aqueous solution confirms that $\{W_{12}\}$ is a salt of strong acid (see Figure S5) in this work. Thus, direct hydrogen bonding between PEG and WO groups of {W₁₂} in aqueous media is also excluded because both PEG and {W₁₂} are hydrogen bonding acceptors without any active hydrogen atoms in their chemical structures. On the other hand, as shown in Figure S6,

thermogravimetric analysis (TGA) of freeze-dried $\{W_{12}\}$ indicates a loss of approximately 2.5 water molecules per $\{W_{12}\}$ at elevated temperature from 100 to 290 °C, suggesting the presence of highly stable water bound with $\{W_{12}\}$. The crystalline structural analysis of $\{W_{12}\}$ by X-ray diffraction as reported previously ^{74,75} also suggests that such interfacial water molecules bind with $\{W_{12}\}$ via hydrogen bonding, for which bound water is considered as a hydrogen bonding donor. Therefore, it becomes reasonable to speculate that the PEG– $\{W_{12}\}$ pairing could occur by water mediation, where bound interfacial water molecules could form hydrogen bonding with both PEG and $\{W_{12}\}$ by sharing one hydration shell at their interfaces, leading to the formation of PEG–water– $\{W_{12}\}$ complexes.

To test our speculation, we adopt a very simple approach of using heavy water, D_2O to examine the phase diagram of PEG- $\{W_{12}\}$ complex coacervation instead of H_2O . As D_2O could form more hydrogen bonds (=3.76) per molecule than that (=3.62) of H_2O , ⁷⁶ D_2O is a stronger hydrogen bonding agent than H_2O . As the phase diagram is shown in Figure 4a,

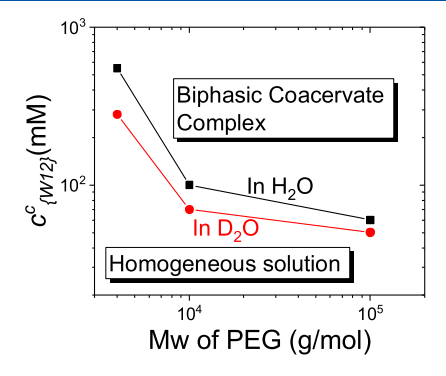


Figure 4. Comparison of the effect of D_2O (red circles) and H_2O (black squares) as aqueous medium on $c_{\{W_{12}\}}^c$ for PEG- $\{W_{12}\}$ complex coacervate formation against PEG M_w at constant initial c_{EG}^i = 1.135 M and c_{LiCl} = 2.0 M.

 $c_{\{W_{12}\}}^c$ shifts to lower concentrations by 20–50% in D₂O than those in H₂O while both c_{PEO}^i and c_{LiCl}^i are kept the same, supporting that D₂O is more effective in mediating PEG– $\{W_{12}\}$ binding via hydrogen bonding than H₂O. Furthermore,

it also confirms that neither vdW nor electrostatic intermolecular interaction is critical for PEG– $\{W_{12}\}$ coacervate formation in that the permittivity of D_2O is the same as that of H_2O , resulting in no change in either vdW or electrostatic interaction. Thus, the effect of D_2O on decreasing $c_{\{W_{12}\}}^c$ for PEG– $\{W_{12}\}$ coacervate formation strongly supports the critical role of water as the hydrogen bond donor for both PEG and $\{W_{12}\}$ to control their coacervation complexation. To the best of our knowledge, it is for the first time that water-mediated organic—inorganic polymeric complex coacervate is developed.

Thermodynamic Origin of PEG-{W₁₂} Complex Coacervation. Last but not least, we investigate the thermodynamic process to drive liquid-liquid separation for PEG-{W₁₂} coacervate formation in aqueous solution. Although the thermodynamic origin of conventional polyelectrolyte complex coacervation remains actively debated in the literature, 79,80 an entropy-driven process with the release of counter ions upon polycation-polyanion pairing has been widely accepted and evidently supported by ITC and other experimental characterizations. 62,81 Our recent study has supported that complex coacervation between zwitterionic polymers and anionic POMs is driven by entropy gain (positive ΔS) by releasing bound anions of polyzwitterions to the supernatant phase.³⁹ In this work, we have also employed ITC to measure the enthalpy change, ΔH upon the liquid-liquid phase separation by mixing {W₁₂} and saltcontaining PEG aqueous solutions. The ΔH of adding $\{W_{12}\}$ -LiCl aqueous solution to the PEG-free LiCl solution of the same c_{LiCl}^{i} as that for PEG-{W₁₂} coacervate formation is measured as the background. As shown in Figure 5, the ΔH of adding aqueous solution of 200 mM {W₁₂} and 2.0 M LiCl to 2.0 M LiCl aqueous solution at 22 °C is only tens of joule per mole $\{W_{12}\}$ and kept nearly constant, suggesting a typical dilution process. However, it is rather surprising to observe the when adding the 200 mM {W₁₂} and 2.0 M LiCl aqueous solution to a solution of 5.0 g/L PEG-100k and 2.0 M LiCl, ΔH remains constant, despite the nearly doubled background value. Moreover, the measured ΔH , after subtracting the background, for mixing PEG and {W₁₂} in LiCl aqueous solution is at least 1 order of magnitude lower than the reported values for conventional polyelectrolyte coacervate formation, 79,81 but in close approximation to the reported

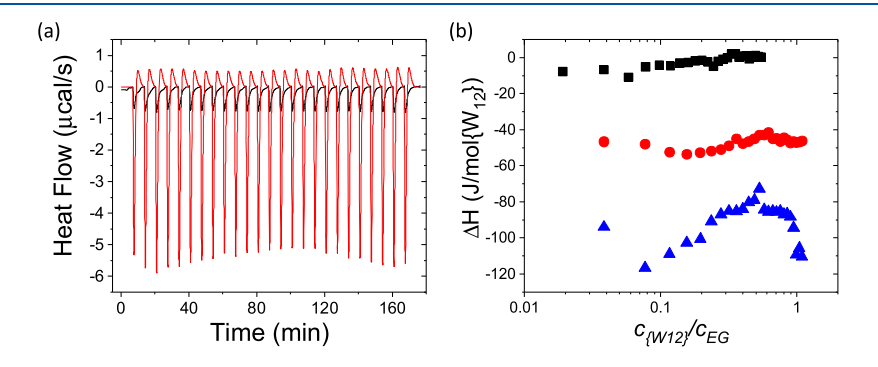
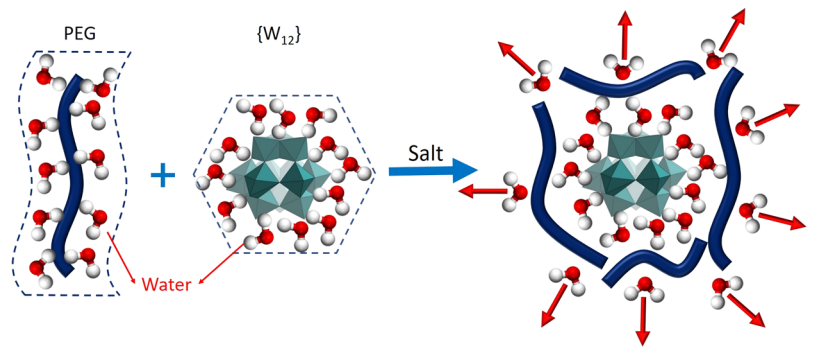


Figure 5. (a) Measured heat flow over time, when consecutive aliquots of each 10 μ L {W₁₂}-LiCl mixed solution of $c_{\text{W}_{12}}^i$ = 200 mM and c_{LiCl} = 2.0 M to PEG-100k and LiCl mixed solution of c_{EG}^i = 0.1136 M and c_{LiCl} = 2.0 M (red line) in comparison to that of adding {W₁₂}-LiCl solution of the same concentrations to 2.0 M LiCl aqueous solution (black line) as control at 22 °C. (b) Measured enthalpy change, ΔH upon the mixing {W₁₂}-LiCl and PEG-100k-LiCl aqueous solutions in H₂O (red circles) and D₂O (blue triangles), for both of which c_{LiCl} = 2.0 M, in comparison to ΔH of injecting {W₁₂}-LiCl solution to PEG-100k-LiCl solution of c_{LiCl} = 1.0 M to form monophasic homogeneous solution of the same c_{EG}^i and $c_{\text{W}_{12}}^i$ (black squares).



Origin of entropy gain: release of hydrated water

Figure 6. Schematic illustration of PEG- $\{W_{12}\}$ binding for complex coacervate formation upon mixing hydrated PEG and $\{W_{12}\}$ in aqueous medium by the release of excess of interfacial hydration water to the bulk solution.

value for $\{W_{12}\}$ -polyzwitterion coacervate formation. It should be noted that the resulting mixture after adding $\{W_{12}\}$ -LiCl (2.0 M) solution with each interval dose of 10 μ L to PEG-LiCl (2.0 M) solution becomes increasingly cloudy, in sharp contrast to the monophasic mixture formed in 1.0 M LiCl aqueous solution with expected little enthalpy change, indicating the commencement of complex coacervation with negligible enthalpy change. Therefore, based on the Gibbs free energy, $\Delta G = \Delta H - T\Delta S$ with negligible ΔH and negative change, $-\Delta G$ for the spontaneous liquid-liquid phase separation, it is clearly inferred that the formation of PEG- $\{W_{12}\}$ coacervate is driven by the entropy gain.

A critical question is then raised from the entropy-driven PEG-{W₁₂} complex coacervation: how is entropy gained upon mixing {W₁₂}-LiCl and PEG-LiCl solutions to result in PEG-{W₁₂} binding and coacervate formation? For conventional coacervate formation between oppositely charged polyelectrolytes, the release of trapped counter ions near the polyelectrolytes mostly accounts for the increased entropy. However, in this work, we have excluded the contribution of LiCl for entropy gain despite its abundant presence in the supernatant phase because strongly water-hydrated LiCl makes it difficult to facilitate the "bridging" of LiCl between anionic {W₁₂} and neutral PEG in aqueous solution. Instead, we speculate that entropy gain results from the release of strongly bound hydrated water from each individual hydration shells of PEG and $\{W_{12}\}\$, where PEG $-H_2O-\{W_{12}\}\$ binding is formed. As both PEG and {W₁₂} are heavily hydrated with several water hydration layers in aqueous solution, we expect that the PEG-{W₁₂} pairing could occur by sharing one water hydration shell while releasing a large amount of excess structured hydration water to the bulk solution as schematically illustrated in Figure 6, leading to considerable entropy gain for biphasic complex coacervation. It is noted that the molar fraction of water in the dense coacervate phase is higher than 90%, thereby unfortunately it becomes difficult to distinguish such bound water from bulk water by current advanced spectroscopy and scattering techniques. A theoretical or computer simulation study of the release of excess interfacial hydration water for complex coacervation between highly hydrophilic polymers and nanocolloids is highly desired.

CONCLUSIONS

In summary, we have successfully demonstrated that water can effectively and directly mediate nonelectrostatic coacervate formation between hydrophilic neutral polymer and inorganic

POM nanoclusters in aqueous solution. Phase diagram of PEG-{W₁₂} aqueous mixtures clearly exhibit the transition from homogeneous solution to liquid-liquid separated complex coacervate when $c_{\{W_{i,j}\}}^c$ is exceeded at a given PEG concentration. Fluorescence microscopy, composition, and SAXS characterization provide comprehensive and convincing evidences of biphasic PEG-{W₁₂} complex coacervates, exhibiting a dense PEG and {W₁₂}-rich aqueous phase and a dilute supernatant phase. It is important to observe that $c_{\{W_n\}}^c$ is much lower in D2O than in H2O and decreases with increasing PEG $M_{\rm w}$, indicating stronger PEG- $\{W_{12}\}$ association in D_2O and with longer PEG chains. Consequently, we exclude the contributions of electrostatic, vdW, and hydrophobic interaction for PEG-{W₁₂} complex coacervates considering the same medium permittivity in D2O and H2O and high hydrophilic nature of both PEG and {W₁₂}. Such unconventional coacervate formation is also confirmed with POMs of different chemical compositions, sizes, and architectural nanostructures. ITC results strongly suggest that PEG-POM complex coacervation is entropy driven. However, the account of releasing counter ion near POMs for entropy gain is excluded in that {W₁₂} demands the presence of Li⁺ counter ions to maintain its electrostatic neutrality. As combined, all the results are pointed to support entropy-driven PEG-H₂O-POM association with the release of excess hydrated water in the hydrogen shells of PEG and POM for coacervate formation. Future research by atomistic dynamics computer simulation could greatly help elucidate the nature of the driving force and the role of structured water for nonelectrostatic complex coacervation.

Such nonelectrostatic organic—inorganic polymeric complex coacervation can be generally extended to highly water-soluble hydrophilic polymers and inorganic nanomaterials. The study of hydrophilic organic—inorganic nanomaterial complexation gives insight to the role of interfacial structured water in many supramolecular assembly processes in nature. For practical applications, it can be developed as a general and simple strategy to build biomimetic hybrid materials with high water content based on self-association in water. The spontaneous aqueous liquid—liquid separation could also open new synthesis routes and nanomanufacturing processes to build new polymer nanocomposites for emerging applications from "green" heterogeneous catalysis, effective ion or proton conducting materials, nanofiltration, and biomedical ramifications.

ASSOCIATED CONTENT

S Supporting Information

The Supporting Information is available free of charge on the ACS Publications website at DOI: 10.1021/acs.macromol.9b01091.

Additional experimental results of POM titration, PEG-POM complex coacervation with different POMs and solution conditions, and SAXS data analysis (PDF)

AUTHOR INFORMATION

Corresponding Authors

*E-mail: jingbenxin@gmail.com (B.J.). *E-mail: yzhu3@wayne.edu (Y.Z.).

ORCID ®

Benxin Jing: 0000-0002-8400-1937 Tianbo Liu: 0000-0002-8181-1790 Yingxi Zhu: 0000-0002-7968-1640

Notes

The authors declare no competing financial interest.

ACKNOWLEDGMENTS

The authors acknowledge the financial support from the National Science Foundation (NSF DMR-1743041 and CHE-1607138) for this work. The authors thank Kehua Lin at the Wayne State University for his experimental assistance, Fangchao Liu and Prof. Guangzhao Mao at the Wayne State University for their TGA support, and Dr. Benjamin Yavitt at the Brookhaven National Laboratory for his assistance in SAXS experimental support. This research used resources and the Complex Materials Scattering (CMS/11-BM) beamline of the National Synchrotron Light Source II, a U.S. Department of Energy (DOE) Office of Science User Facility operated for the DOE Office of Science by Brookhaven National Laboratory under contract no. DE-SC0012704.

REFERENCES

- (1) Ball, P. Water as an Active Constituent in Cell Biology. Chem. Rev. 2008, 108, 74–108.
- (2) Ball, P. Water is an active matrix of life for cell and molecular biology. *Proc. Natl. Acad. Sci. U.S.A.* **2017**, *114*, 13327–13335.
- (3) García-Sosa, A. T. Hydration Properties of Ligands and Drugs in Protein Binding Sites: Tightly-Bound, Bridging Water Molecules and Their Effects and Consequences on Molecular Design Strategies. *J. Chem. Inf. Model.* **2013**, *53*, 1388–1405.
- (4) Davey, C. A.; Sargent, D. F.; Luger, K.; Maeder, A. W.; Richmond, T. J. Solvent Mediated Interactions in the Structure of the Nucleosome Core Particle at 1.9 Å Resolution. *J. Mol. Biol.* **2002**, 319, 1097–1113.
- (5) Reichmann, D.; Phillip, Y.; Carmi, A.; Schreiber, G. On the Contribution of Water-Mediated Interactions to Protein-Complex Stability. *Biochemistry* **2008**, *47*, 1051–1060.
- (6) Levinson, N. M.; Boxer, S. G. A conserved water-mediated hydrogen bond network defines bosutinib's kinase selectivity. *Nat. Chem. Biol.* **2014**, *10*, 127–132.
- (7) Julius, K.; Weine, J.; Berghaus, M.; König, N.; Gao, M.; Latarius, J.; Paulus, M.; Schroer, M. A.; Tolan, M.; Winter, R. Water-Mediated Protein-Protein Interactions at High Pressures are Controlled by a Deep-Sea Osmolyte. *Phys. Rev. Lett.* **2018**, *121*, 038101.
- (8) Setny, P.; Wiśniewska, M. D. Water-mediated conformational preselection mechanism in substrate binding cooperativity to protein kinase A. *Proc. Natl. Acad. Sci. U.S.A.* **2018**, *115*, 3852–3857.
- (9) Papoian, G. A.; Ulander, J.; Wolynes, P. G. Role of Water Mediated Interactions in Protein—Protein Recognition Landscapes. *J. Am. Chem. Soc.* **2003**, 125, 9170—9178.

(10) Thirumalai, D.; Reddy, G.; Straub, J. E. Role of Water in Protein Aggregation and Amyloid Polymorphism. *Acc. Chem. Res.* **2012**, 45, 83–92.

- (11) Wang, Y.; Von Euw, S.; Fernandes, F. M.; Cassaignon, S.; Selmane, M.; Laurent, G.; Pehau-Arnaudet, G.; Coelho, C.; Bonhomme-Coury, L.; Giraud-Guille, M.-M.; Babonneau, F.; Azaïs, T.; Nassif, N. Water-mediated structuring of bone apatite. *Nat. Mater.* **2013**, *12*, 1144.
- (12) Wilson, E. E.; Awonusi, A.; Morris, M. D.; Kohn, D. H.; Tecklenburg, M. M. J.; Beck, L. W. Three Structural Roles for Water in Bone Observed by Solid-State NMR. *Biophys. J.* **2006**, *90*, 3722–3731.
- (13) Umena, Y.; Kawakami, K.; Shen, J.-R.; Kamiya, N. Crystal structure of oxygen-evolving photosystem II at a resolution of 1.9 Å. *Nature* **2011**, 473, 55.
- (14) Brunk, E.; Arey, J. S.; Rothlisberger, U. Role of Environment for Catalysis of the DNA Repair Enzyme MutY. J. Am. Chem. Soc. 2012, 134, 8608–8616.
- (15) Johnson, R. S.; Yamazaki, T.; Kovalenko, A.; Fenniri, H. Molecular Basis for Water-Promoted Supramolecular Chirality Inversion in Helical Rosette Nanotubes. *J. Am. Chem. Soc.* **2007**, 129, 5735–5743.
- (16) Dong, S.; Leng, J.; Feng, Y.; Liu, M.; Stackhouse, C. J.; Schönhals, A.; Chiappisi, L.; Gao, L.; Chen, W.; Shang, J.; Jin, L.; Qi, Z.; Schalley, C. A. Structural water as an essential comonomer in supramolecular polymerization. *Sci. Adv.* **2017**, *3*, eaao0900.
- (17) Oshovsky, G. V.; Reinhoudt, D. N.; Verboom, W. Supramolecular Chemistry in Water. *Angew. Chem., Int. Ed.* **2007**, 46, 2366–2393.
- (18) Mitchell, H. H.; Hamilton, T. S.; Steggerda, F. R.; Bean, H. W. The Chemical Composition Of The Adult Human Body And Its Bearing On The Biochemistry Of Growth. *J. Biol. Chem.* **1945**, *158*, 625–637.
- (19) Shin, Y.; Brangwynne, C. P. Liquid phase condensation in cell physiology and disease. *Science* **2017**, *357*, eaaf4382.
- (20) Stewart, R. J.; Wang, C. S.; Song, I. T.; Jones, J. P. The role of coacervation and phase transitions in the sandcastle worm adhesive system. *Adv. Colloid Interface Sci.* **2017**, 239, 88–96.
- (21) Zhao, H.; Sun, C.; Stewart, R. J.; Waite, J. H. Cement Proteins of the Tube-building Polychaete Phragmatopoma californica. *J. Biol. Chem.* **2005**, 280, 42938–42944.
- (22) Stewart, R. J.; Ransom, T. C.; Hlady, V. Natural Underwater Adhesives. J. Polym. Sci., Part B: Polym. Phys. 2011, 49, 757-771.
- (23) Jia, T. Z.; Hentrich, C.; Szostak, J. W. Rapid RNA Exchange in Aqueous Two-Phase System and Coacervate Droplets. *Origins Life Evol. Biospheres* **2014**, *44*, 1–12.
- (24) Jia, T. Z.; Fahrenbach, A. C.; Kamat, N. P.; Adamala, K. P.; Szostak, J. W. Oligoarginine Peptides Slow Strand Annealing and Assist Non-enzymatic RNA Replication. *Nat. Chem.* **2016**, *8*, 915–921.
- (25) Lee, B. P.; Messersmith, P. B.; Israelachvili, J. N.; Waite, J. H. Mussel-Inspired Adhesives and Coatings. In *Annual Review of Materials Research*; Clarke, D. R., Fratzl, P., Eds., 2011; Vol. 41, pp 99–132.
- (26) Priftis, D.; Leon, L.; Song, Z.; Perry, S. L.; Margossian, K. O.; Tropnikova, A.; Cheng, J.; Tirrell, M. Self-Assembly of α -Helical Polypeptides Driven by Complex Coacervation. *Angew. Chem., Int. Ed.* **2015**, *54*, 11128–11132.
- (27) Priftis, D.; Leon, L.; Song, Z.; Perry, S. L.; Margossian, K. O.; Tropnikova, A.; Cheng, J.; Tirrell, M. Self-Assembly of α -Helical Polypeptides Driven by Complex Coacervation. *Angew. Chem.* **2015**, 127, 11280–11284.
- (28) Li, L.; Yan, B.; Yang, J.; Chen, L.; Zeng, H. Novel Mussel-Inspired Injectable Self-Healing Hydrogel with Anti-Biofouling Property. *Adv. Mater.* **2015**, *27*, 1294–1299.
- (29) Croguennec, T.; Tavares, G. M.; Bouhallab, S. Heteroprotein complex coacervation: A generic process. *Adv. Colloid Interface Sci.* **2017**, 239, 115–126.

(30) Mason, A. F.; Buddingh', B. C.; Williams, D. S.; van Hest, J. C. M. Hierarchical Self-Assembly of a Copolymer-Stabilized Coacervate Protocell. *J. Am. Chem. Soc.* **2017**, *139*, 17309–17312.

- (31) Yin, P.; Wu, B.; Mamontov, E.; Daemen, L. L.; Cheng, Y.; Li, T.; Seifert, S.; Hong, K.; Bonnesen, P. V.; Keum, J. K.; Ramirez-Cuesta, A. J. X-ray and Neutron Scattering Study of the Formation of Core—Shell-Type Polyoxometalates. *J. Am. Chem. Soc.* **2016**, *138*, 2638–2643.
- (32) Comert, F.; Dubin, P. L. Liquid-Liquid and Liquid-Solid Phase Separation in Protein-Polyelectrolyte Systems. *Adv. Colloid Interface Sci.* **2017**, 239, 213–217.
- (33) Kizilay, E.; Kayitmazer, A. B.; Dubin, P. L. Complexation and Coacervation of Polyelectrolytes With Oppositely Charged Colloids. *Adv. Colloid Interface Sci.* **2011**, *167*, 24–37.
- (34) Zhao, M.; Eghtesadi, S. A.; Dawadi, M. B.; Wang, C.; Huang, S.; Seymore, A. E.; Vogt, B. D.; Modarelli, D. A.; Liu, T.; Zacharia, N. S. Partitioning of Small Molecules in Hydrogen-Bonding Complex Coacervates of Poly(acrylic acid) and Poly(ethylene glycol) or Pluronic Block Copolymer. *Macromolecules* 2017, 50, 3818–3830.
- (35) Nam, H. G.; Nam, M. G.; Yoo, P. J.; Kim, J.-H. Hydrogen bonding-based strongly adhesive coacervate hydrogels synthesized using poly(N-vinylpyrrolidone) and tannic acid. *Soft Matter* **2019**, *15*, 785–791.
- (36) Kim, S.; Huang, J.; Lee, Y.; Dutta, S.; Yoo, H. Y.; Jung, Y. M.; Jho, Y.; Zeng, H.; Hwang, D. S. Complexation and Coacervation of Like-charged Polyelectrolytes Inspired by Mussels. *Proc. Natl. Acad. Sci. U.S.A.* **2016**, *113*, E847–E853.
- (37) Valley, B.; Jing, B.; Ferreira, M.; Zhu, Y. Rapid and Efficient Coacervate Extraction of Cationic Industrial Dyes from Wastewater. ACS Appl. Mater. Interfaces 2019, 11, 7472–7478.
- (38) Jing, B.; Xu, D.; Wang, X.; Zhu, Y. Multiresponsive, Critical Gel Behaviors of Polyzwitterion—Polyoxometalate Coacervate Complexes. *Macromolecules* **2018**, *51*, 9405—9411.
- (39) Jing, B.; Qiu, J.; Zhu, Y. Organic-inorganic macroion coacervate complexation. *Soft Matter* **2017**, *13*, 4881–4889.
- (40) Crowley, J. K. Visible and near-infrared (0.4–2.5 μm) reflectance spectra of Playa evaporite minerals. J. Geophys. Res., [Solid Earth Planets] 1991, 96, 16231–16240.
- (41) Heiri, O.; Lotter, A. F.; Lemcke, G. Loss on ignition as a method for estimating organic and carbonate content in sediments: reproducibility and comparability of results. *J. Paleolimnol.* **2001**, 25, 101–110.
- (42) Laage, D.; Elsaesser, T.; Hynes, J. T. Water Dynamics in the Hydration Shells of Biomolecules. *Chem. Rev.* **2017**, *117*, 10694–10725.
- (43) Stack, A. G.; Borreguero, J. M.; Prisk, T. R.; Mamontov, E.; Wang, H.-W.; Vlcek, L.; Wesolowski, D. J. Precise determination of water exchanges on a mineral surface. *Phys. Chem. Chem. Phys.* **2016**, *18*, 28819–28828.
- (44) Yan, C.; Nishida, J.; Yuan, R.; Fayer, M. D. Water of Hydration Dynamics in Minerals Gypsum and Bassanite: Ultrafast 2D IR Spectroscopy of Rocks. *J. Am. Chem. Soc.* **2016**, *138*, 9694–9703.
- (45) Lüsse, S.; Arnold, K. The Interaction of Poly(ethylene glycol) with Water Studied by1H and 2H NMR Relaxation Time Measurements. *Macromolecules* **1996**, 29, 4251–4257.
- (46) Khutoryanskiy, V. V.; Dubolazov, A. V.; Nurkeeva, Z. S.; Mun, G. A. pH Effects in the Complex Formation and Blending of Poly(acrylic acid) with Poly(ethylene oxide). *Langmuir* **2004**, *20*, 3785–3790.
- (47) Bailey, F. E., Jr.; Lundberg, R. D.; Callard, R. W. Some factors affecting the molecular association of poly(ethylene oxide) and poly(acrylic acid) in aqueous solution. *J. Polym. Sci., Part A: Gen. Pap.* **1964**, *2*, 845–851.
- (48) Liu, T. Hydrophilic Macroionic Solutions: What Happens When Soluble Ions Reach the Size of Nanometer Scale? *Langmuir* **2010**, 26, 9202–9213.
- (49) Long, D.-L.; Burkholder, E.; Cronin, L. Polyoxometalate Clusters, Nanostructures and Materials: From Self Assembly to Designer Materials and Devices. *Chem. Soc. Rev.* **2007**, *36*, 105–121.

- (50) Oleinikova, A.; Weingärtner, H.; Chaplin, M.; Diemann, E.; Bögge, H.; Müller, A. Self-Association Based on Interfacial Structured Water Leads to {Mo154}≈1165 Super Clusters: A Dielectric Study. *ChemPhysChem* **2007**, *8*, 646−649.
- (51) Shivaiah, V.; Das, S. K. Polyoxometalate-Supported Transition Metal Complexes and Their Charge Complementarity: Synthesis and Characterization of $[M(OH)_6Mo_6O_{18}\{Cu(Phen)(H_2O)_2\}_2][M-(OH)_6Mo_6O_{18}\{Cu(Phen)(H_2O)\ Cl\}_2]\cdot SH_2O\ (M=Al^{3+},\ Cr^{3+}).$ Inorg. Chem. 2005, 44, 8846–8854.
- (52) Garcia-Ratés, M.; Miró, P.; Poblet, J. M.; Bo, C.; Avalos, J. B. Dynamics of Encapsulated Water inside Mo132 Cavities. *J. Phys. Chem. B* **2011**, *115*, 5980–5992.
- (53) LMT Density. https://www.lmtliquid.com/density-calculator.html (accessed October 2018).
- (54) Gonzalez-Tello, P.; Camacho, F.; Blazquez, G. Density and Viscosity of Concentrated Aqueous Solutions of Polyethylene Glycol. *J. Chem. Eng. Data* **1994**, *39*, 611–614.
- (55) Water analysis. In *Practical Environmental Analysis*; Radojević, M., Bashkin, V. N., Eds.; The Royal Society of Chemistry, 1999; pp 138–273.
- (56) Yoder, L. Adaptation of the Mohr Volumetric Method to General Determinations of Chlorine. *J. Ind. Eng. Chem.* **1919**, *11*, 755. (57) Kehl, K. G.; Meyer, V. R. Argentometric Titration for the Determination of Liquid Chromatographic Injection Reproducibility.

Anal. Chem. 2001, 73, 131-133.

- (58) Chollakup, R.; Beck, J. B.; Dirnberger, K.; Tirrell, M.; Eisenbach, C. D. Polyelectrolyte Molecular Weight and Salt Effects on the Phase Behavior and Coacervation of Aqueous Solutions of Poly(acrylic acid) Sodium Salt and Poly(allylamine) Hydrochloride. *Macromolecules* **2013**, *46*, 2376–2390.
- (59) Spruijt, E.; Westphal, A. H.; Borst, J. W.; Cohen Stuart, M. A.; van der Gucht, J. Binodal Compositions of Polyelectrolyte Complexes. *Macromolecules* **2010**, *43*, 6476–6484.
- (60) Lou, J.; Friedowitz, S.; Qin, J.; Xia, Y. Tunable Coacervation of Well-Defined Homologous Polyanions and Polycations by Local Polarity. ACS Cent. Sci. 2019, 5, 549–557.
- (61) Sing, C. E. Development of the modern theory of polymeric complex coacervation. *Adv. Colloid Interface Sci.* **2017**, 239, 2–16.
- (62) Li, L.; Srivastava, S.; Andreev, M.; Marciel, A. B.; de Pablo, J. J.; Tirrell, M. V. Phase Behavior and Salt Partitioning in Polyelectrolyte Complex Coacervates. *Macromolecules* **2018**, *51*, 2988–2995.
- (63) Zhang, P.; Shen, K.; Alsaifi, N. M.; Wang, Z.-G. Salt Partitioning in Complex Coacervation of Symmetric Polyelectrolytes. *Macromolecules* **2018**, *51*, 5586–5593.
- (64) Albertsson, P.-Å.; Tjerneld, F. [1] Phase diagrams. In *Methods in Enzymology*; Academic Press, 1994; Vol. 228, pp 3–13.
- (65) Johansson, H.-O.; Feitosa, E.; Junior, A. P. Phase Diagrams of the Aqueous Two-Phase Systems of Poly(ethylene glycol)/Sodium Polyacrylate/Salts. *Polymers* **2011**, *3*, 587.
- (66) Buchecker, T.; Le Goff, X.; Naskar, B.; Pfitzner, A.; Diat, O.; Bauduin, P. Polyoxometalate/Polyethylene Glycol Interactions in Water: From Nanoassemblies in Water to Crystal Formation by Electrostatic Screening. *Chem.—Eur. J.* 2017, 23, 8434–8442.
- (67) Mertens, H. D. T.; Svergun, D. I. Structural characterization of proteins and complexes using small-angle X-ray solution scattering. *J. Struct. Biol.* **2010**, *172*, 128–141.
- (68) Rambo, R. P.; Tainer, J. A. Characterizing flexible and intrinsically unstructured biological macromolecules by SAS using the Porod-Debye law. *Biopolymers* **2011**, *95*, 559–571.
- (69) Doniach, S. Changes in Biomolecular Conformation Seen by Small Angle X-ray Scattering. *Chem. Rev.* **2001**, *101*, 1763–1778.
- (70) Putnam, C. D. Guinier peak analysis for visual and automated inspection of small-angle X-ray scattering data. *J. Appl. Crystallogr.* **2016**, *49*, 1412–1419.
- (71) André Guinier, G. F. Small-Angle Scattering of X-rays; John Wiley and Sons: New York, 1955.
- (72) Petoukhov, M. V.; Konarev, P. V.; Kikhney, A. G.; Svergun, D. I. ATSAS 2.1—towards automated and web-supported small-angle scattering data analysis. *J. Appl. Crystallogr.* **2007**, *40*, s223—s228.

Macromolecules

(73) Sprangers, C. R.; Marmon, J. K.; Duncan, D. C. Where Are the Protons in α - $[H_xW_{12}O_{40}]_{(8-x)}$ (x = 2-4)? *Inorg. Chem.* **2006**, 45, 9628–9630.

- (74) Christian, J. B.; Whittingham, M. S. Structural study of ammonium metatungstate. *J. Solid State Chem.* **2008**, *181*, 1782–1791.
- (75) Hunyadi, D.; Sajó, I.; Szilágyi, I. M. Structure and thermal decomposition of ammonium metatungstate. *J. Therm. Anal. Calorim.* **2014**, *116*, 329–337.
- (76) Soper, A. K.; Benmore, C. J. Quantum Differences between Heavy and Light Water. *Phys. Rev. Lett.* **2008**, *101*, 065502.
- (77) Israelachvili, J. N. 2—Thermodynamic and Statistical Aspects of Intermolecular Forces. In *Intermolecular and Surface Forces*, 3rd ed.; Israelachvili, J. N., Ed.; Academic Press: San Diego, 2011; pp 23–51.
- (78) Vidulich, G. A.; Evans, D. F.; Kay, R. L. The dielectric constant of water and heavy water between 0° and 40°. *J. Phys. Chem.* **1967**, 71, 656–662.
- (79) Kayitmazer, A. B. Thermodynamics of Complex Coacervation. *Adv. Colloid Interface Sci.* **2017**, 239, 169–177.
- (80) Liu, X.; Chapel, J.-P.; Schatz, C. Structure, thermodynamic and kinetic signatures of a synthetic polyelectrolyte coacervating system. *Adv. Colloid Interface Sci.* **2017**, 239, 178–186.
- (81) Fu, J.; Schlenoff, J. B. Driving Forces for Oppositely Charged Polyion Association in Aqueous Solutions: Enthalpic, Entropic, but Not Electrostatic. *J. Am. Chem. Soc.* **2016**, *138*, 980–990.